Demonstration of TNSA proton radiography on the National Ignition Facility Advanced Radiographic Capability (NIF-ARC) Laser

R.A. Simpson[1,2], D.A. Mariscal[1], J. Kim[1,6], G.G. Scott[1], G.J. Williams[1], E. Grace[1,5], C. McGuffey[6,7], S. Wilks[1], A. Kemp[1], N. Lemos[1], B.Z. Djordjevic[1], E. Folsom[1], D. Kalantar[1], R. Zacharias[1], B. Pollock[1], J. Moody[1], F. Beg[6], A. Morace[9], N. Iwata[9], Y. Sentoku[9], M. J.-E Manuel[7],M. Mauldin[7], M. Quinn[7], and K. Youngblood[7] M. Gatu-Johnson[3], B. Lahmann[3], C. Haefner[8], D. Neely[4], and T. Ma[1]

[1]Lawrence Livermore National Laboratory, Livermore CA USA
[2]Department of Nuclear Science and Engineering, Massachusetts Institute of Technology, Cambridge MA USA
[3]Plasma Science and Fusion Center, Massachusetts Institute of Technology, Cambridge MA USA
[4]Central Laser Facility, Rutherford Appleton Laboratory, Didcot UNITED KINGDOM
[5]School of Physics, The Georgia Institute of Technology, Atlanta, GA USA
[6]Center for Energy Research, University of California San Diego, La Jolla, CA USA
[7]General Atomics, San Diego, CA USA
[8]Fraunhofer Institute of Laser Technology. Aachen GERMANY
[9]Institute of Laser Engineering, University of Osaka, Osaka JAPAN

E-mail: razzy@mit.edu

Abstract. Proton radiography using short-pulse laser drivers is an important tool in high-energy density (HED) science for dynamically diagnosing key characteristics in plasma interactions. Here we detail the first demonstration of target-normal sheath acceleration (TNSA)-based proton radiography the NIF-ARC laser system aided by the use of compound parabolic concentrators (CPCs). The multi-kJ energies available at the NIF-ARC laser allows for a high-brightness proton source for radiography and thus enabling a wide range of applications in HED science. In this demonstration, proton radiography of a physics package was performed and this work details the spectral properties of the TNSA proton probe as well as description of the resulting radiography quality.

1. Introduction

Proton radiography has long been a crucial tool in high-energy density (HED) science for probing and characterizing HED plasmas. Proton radiography sources used in HED applications have chiefly been produced through either a fusion capsule implosion [1, 2, 3], which acts as a spatially isotropic monoenergetic D-D (3.02 MeV) and D-^{3}He (14.7 MeV) proton source, or through the target-normal sheath acceleration (TNSA) mechanism, where the proton source has a characteristic broadband exponential spectrum and beam-like structure. [4, 5] TNSA proton sources for radiography purposes have the added benefit of being able to perform time-resolved radiography of plasma interactions, thus providing the ability to create a "movie" of plasma phenomena. These TNSA proton sources have been demonstrated across a wide variety of laser systems globally [6, 7, 8, 9] and utilized for applications ranging from probing of magnetic reconnection experiments [10] to diagnosing of electric and magnetic fields through deflectrometry [11].

The Advanced Radiographic Capability (NIF-ARC) laser at the National Ignition Facility (NIF) is a petawatt-class, multi-kilojoule, multi-ps laser that typically operates at laser intensities of $\sim 10^{18}$ W/cm^2 [12]. The NIF-ARC system is composed of four separate beamlets that can be individually timed and pointed, thus allowing for flexible applications in high-energy density science. For instance, one could stack pulses temporally in order to create long time-scale proton probes or use multiple beamlets simultaneously along different lines of sight to achieve tomography of HED plasmas. While the primary initial purpose of the NIF-ARC system was to provide x-ray backlighter capabilities for inertial confinement fusion (ICF) implosions driven by the long-pulse NIF platform, recent results using the NIF-ARC have shown promising avenues for its use as a proton backlighter through the target-normal sheath acceleration (TNSA) mechanism. These series of proton TNSA experiments on the NIF-ARC have demonstrated proton energies that exceed that of established proton scaling laws, despite the system's quasi-relativistic laser intensities [13]. In these prior experiments, flat titanium foils (33-microns thick) were irradiated with either 1.6 or 10 ps pulses at intensities of 1.5×10^{18} W/cm^2 and 9.1×10^{17} W/cm^2, respectively, and were found to have proton energies of 18 and 14 MeV, respectively. While these maximum proton energies are impressive given the relatively low laser intensities achievable during standard operation of the NIF-ARC, higher energy protons would widen the application space for proton radiography. For instance, these energies may be appropriate for diagnosing electric and magnetic fields, but they are not quite high enough to radiograph dense targets, such as inertial confinement fusion implosions, which need proton energies in excess of $\sim$30 MeV [4]. However, recent experiments utilizing innovative compound parabolic concentrators (CPC) targets have demonstrated the ability to increase the effective intensity of the NIF-ARC laser substantially ($\sim 10\times$) beyond its nominal value, thus allowing the potential of an even more energetic and brighter proton TNSA source. CPCs are optical devices with a parabolic shape that allow for all laser light that enters

the cone entrance to be concentrated to the tip of the cone and thereby increase the effective intensity of laser pulses that may have larger and more diffuse spots. [14] In addition, the CPCs allow for easier pointing stability, since all beams that enter the entrance of the cone (which typically have entrance radii of 100s of microns) are reflected to the tip. These cones are defined by their tip diameter, which is typically in the 10s of microns, and the cone material, which is often a plastic or plastic coated with high-Z metals like gold. The NIF-ARC laser system has relatively large focal spots ($\sim$10s of microns) compared to other petawatt class lasers and due to this spot size, the intensities of the systems are limited (10^{18} W/cm^2). Therefore, the CPCs present a useful tool to access physics with the NIF-ARC laser that would otherwise only be achievable with much higher intensities without major facility changes.

The two recent innovations provided increased motivation for investigating the NIF-ARC platform as a viable source for proton TNSA radiography in earnest. In addition, while there has been previous work on using CPCs on the NIF-ARC [15] and other shorter-pulse facilities [16], there had not yet been a demonstration of this capability on the NIF-ARC for the purposes of proton acceleration. The prospect of a high-flux proton radiographical source, given the multi-kJ laser energies coupled with the 10s of MeV proton energies already demonstrated on the NIF-ARC, make it an attractive source for proton radiography and deflectrometry for various and unique applications in high-energy density science. In addition, the large focal spot (10s of microns) and long pulse durations (multi-ps) of the NIF-ARC, are unique laser parameter characteristics when compared to other petawatt class facilities and the use of CPCs on this class of facilities had not yet been demonstrated. The results shown in this paper are a first step in understanding the physics of multi-ps interactions with a complex CPC target and their utility in generating protons.

While the focus of using this source is for proton radiography, this platform may also be used for stopping power measurements [17] or experiments in isochoric heating [18, 19]. In addition, further work might be warranted to apply CPCs for applications to TNSA with heavier ions such as deuterons. This could be a useful extension of this capability as a first-stage to a "pitcher-catcher" system where high-energy TNSA deuterons and protons are directed into a secondary (lithium or beryllium) target to create a highly directional neutron source [20].

In this work, a TNSA proton probe was demonstrated on the NIF-ARC and used to radiograph a physics package aimed at studying isochoric heating. The focus of this paper will be only on characterizing the proton probe as a radiography source and the details and findings of the isochoric heating experiment will be left for a following publication.

2. Experimental Methodology

Two shots were performed on NIF-ARC with the goal of demonstrating proton radiography of a copper puck that was isochorically heated with a separate TNSA-

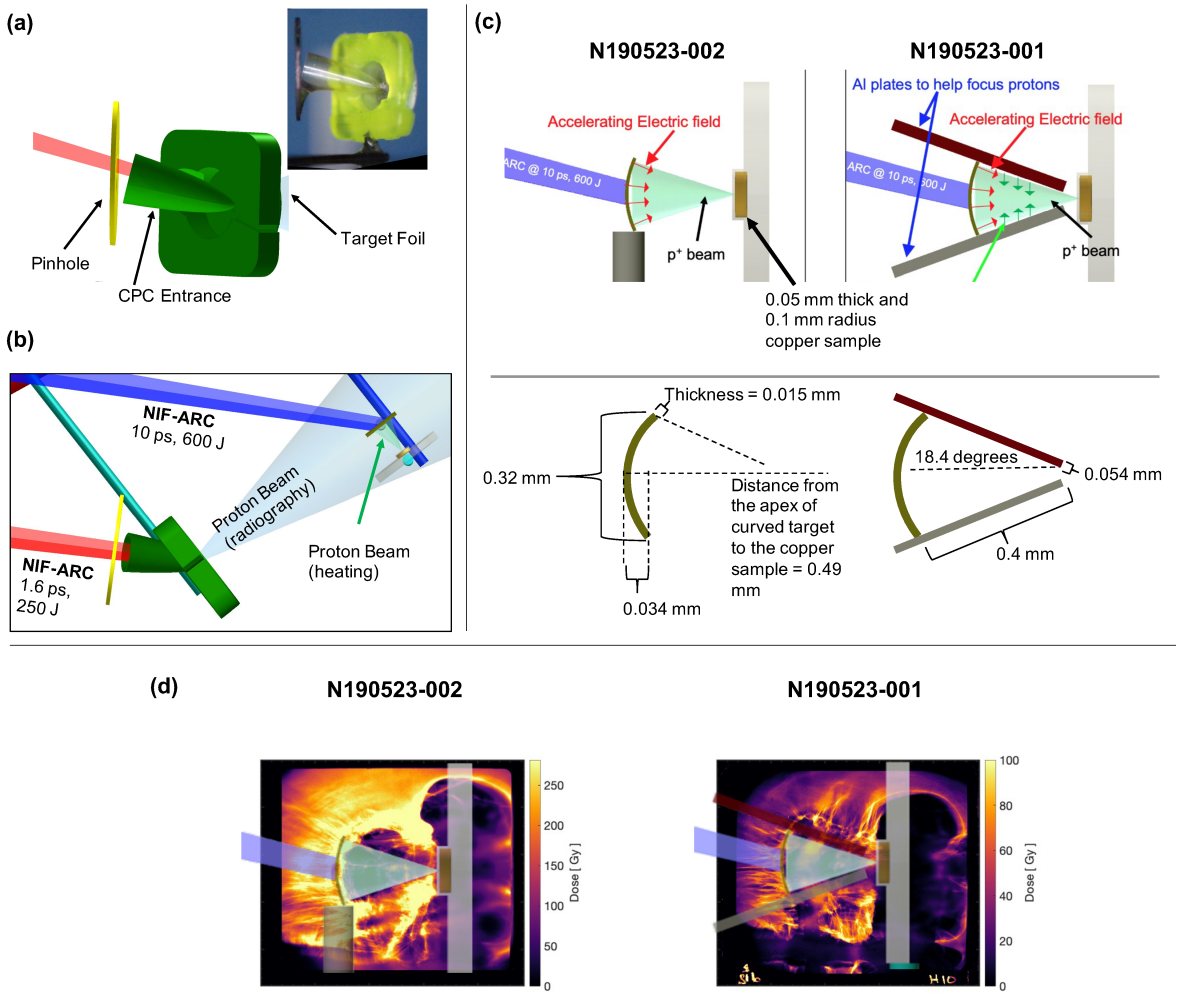

Figure 1. (a) shows a 3-D rendering of the CPC cone used on this experiment and inset is a real picture of one of the cones used on these shots. The green housing holds both the CPC in correct orientation and position and target foil that follows it. In order to mitigate risk to the NIF-ARC due to back-reflection from the target, a plate with an aperture was added shown in (a) such that the NIF-ARC laser would not see a normal surface. (b) shows a polar view of the entire experimental setup. One NIF-ARC beamlet was used to generate a proton probe for radiography and another was used to generate a proton source for heating of the radiography physics package. (c) shows the physics package used for both shots with and without the focusing wedge as well as the geometry of the proton heating target and aluminium focusing wedge structure. (d) shows example RCF layers from both shots with the experimental geometry overlaid on top.

generated proton source. The configuration of the experiment allowed for the characterization of the proton radiography source with the CPC cone while also further investigating a focusing isochoric heating platform, which was recently demonstrated on the OMEGA-EP facility in McGuffey *et al.* [21]. In this OMEGA-EP experiment, TNSA protons were focused using wedged aluminium plates onto a copper puck. In that

work, the wedge structure was found to increase the proton flux at the wedge center by five-fold when compared to heating without the wedge. Using this experiment as a model, a 10-ps, 600 J NIF-ARC beamlet was directed onto a 15-micron-thick curved foil to create a flux of protons for the purpose of heating. Like the McGuffey *et al.* experiment, one shot (Shot ID: N190523-001) utilized an aluminium wedge to provide an inward electric field for proton focusing and the other shot had no wedge structure (Shot ID: N190523-002). This physics package was then radiographed with a separate TNSA proton source.

To generate the radiography proton source, a CPC with a 50 μm opening at the tip was used to couple the energy from a 1.6-ps 250 J NIF-ARC beamlet onto a 15-micron-thick flat titanium foil. On N190523-001 and N190523-002, the NIF-ARC beamlet had a focal spot size of 60 microns and 53 microns respectively. The time delay between this laser pulse to generate the proton probe and the laser pulse to generate protons for heating was measured using the Dilation X-ray Imager (DIXI) and the delay was roughly 50 ps. [22] The CPC was plastic (CH) and had a wall thickness of 25 μm and entrance radius of 242 μm. Figure 1(a) shows a 3-D rendering of the CPC cone used on both shots. The CPC eases alignment accuracy restrictions since the beam is reflected to tip as long as it enters the cone entrance. While the NIF-ARC has a pointing uncertainty of roughly 35 microns, the entrance radii of CPCs used on these shots was much greater than that and therefore the CPCs allow for better pointing stability. Figure 1(b) shows a polar view of the experimental setup and Figure 1(c) includes geometric details about the radiography physics package. Figure 1(d), shows example RCF layers from these two shot days, with a schematic of the experimental geometry overlaid on top to show the approximate orientation of the physics package.

The radiography plane was based on radiochromic film (RCF) and its placement relative to the physics package yielded an imaging magnification of 33. The radiochromic film package was composed of multiple layers of film and aluminium filters and since TNSA sources are characteristically emitted with a broadband exponential spectrum, using the time-of-flight of protons with different energies coupled with the known stopping power of protons in different layers of the RCF pack allows for a discretized "movie" of the heating of the physics package. For Shot ID: N190523-001, the RCF stack was designed with 10 layers of HD-V2 for the front of the pack and 12 layers MD-55 for the back of the package. The MD-55 was used because it has a higher sensitivity, ensuring detection of higher energy protons that are produced in relatively lower numbers. For Shot ID: N190523-002, the RCF pack was slightly modified with two fewer layers of MD-55 resulting in 10 layers of HD-V2 and 10 layers of MD-55 film. For both RCF packs, the temporal resolution was an average of 20-ps across the pack and they were designed to measure maximum proton energies of 24 (Shot ID: N190523-001) or 26 MeV (Shot ID: N190523-001) over roughly $\sim$70 ps. Therefore, the RCF pack allowed for not only a radiography movie of the dynamics of the physics package for isochoric heating, but also characterization of the spectrum of the CPC-aided TNSA proton source.

3. Experimental Results

Figure 2 shows the sequence of images recorded with each RCF stack from both shots on the NIF-ARC platform. RCF layers were scanned on an EPSON EXPRESSION 10000 scanner with a resolution of 600 dots-per-inch (DPI) and are shown in units of optical density (OD). Qualitatively, for both shots, the proton probe source has a signal up to the last layer of RCF at levels 5-10 $\times$ higher than the background, and thus it is likely that the true maximum proton energy is greater than 26 MeV. This exceeds previous TNSA experiments on the NIF-ARC without the CPC cone by more than at least 8 MeV thus demonstrating the effectiveness of the CPCs in enhancing the coupling of the NIF-ARC to the target to generate higher proton energies. These enhanced proton energies may also be due to a larger population of super-ponderomotive electrons that establish the accelerating sheath field. Recent simulation work [23], has shown that the long pulse duration and large focal spot of the NIF-ARC means that there is more pre-plasma blow-off generated within the CPC due to interaction of the beginning of the laser pulse with cone walls. This in turn generates a longer scale length plasma with which the rest of the laser pulse can interact with, thus generating super-ponderomotive electrons via direct laser acceleration.

3.1. Spectral Characterization of Proton Probe

To characterize the spectrum of the proton probe, the RCF diagnostic was utilized. For the RCF stack, the proton dose on each film was summed with the assumption that the density variations and field variations due to the physics package were small enough that the entire proton probe source was captured on the RCF. In this way, a discrete proton probe spectrum can be captured on the RCF (along the probe laser axis). Figure 3(a) shows the relative spectrum for the two NIF-ARC shots (with and without the wedge). To compute absolute proton values, a calibration developed by G.G. Scott [25] for this EPSON EXPRESSION 10000 scanner was utilized. However, this calibration is only for HD-V2 films and thus analysis is only shown in Figure 3(a) for the first 10 layers in the pack. In addition to the maximum proton energy, the spectral slope temperature also a further metric to characterize the spectrum. This is achieved by fitting the spectrum with an exponential of the form $\exp(-E_{MEV}/T_{MeV})$, where T_{MeV} is taken as the slope temperature of the spectrum. In Figure 3(a), fitting the RCF spectrum yields a consistent proton slope temperature between both shots of 3.1 MeV. From these dose measurements on each layer of the RCF, a spectrum in terms of the more familiar units of protons/MeV can be inferred using the known response function of the RCF stack. [26]. Assuming a Boltzmann distribution of the form, $\frac{dN}{dE} = (N/T) * \exp(-E/T)$, parameterized by N, the proton number, and T the temperature of the spectrum in MeV, the dose (D) on each layer of RCF can be calculated using the response function (R) with the equation $D = \int \frac{dN}{dE} R dE$. Therefore, using this the error between the inferred dose for a given spectrum and the measured dose can be minimized to find parameters, N and T to define the spectrum that best captures the measured dose.

(a) N190523-001

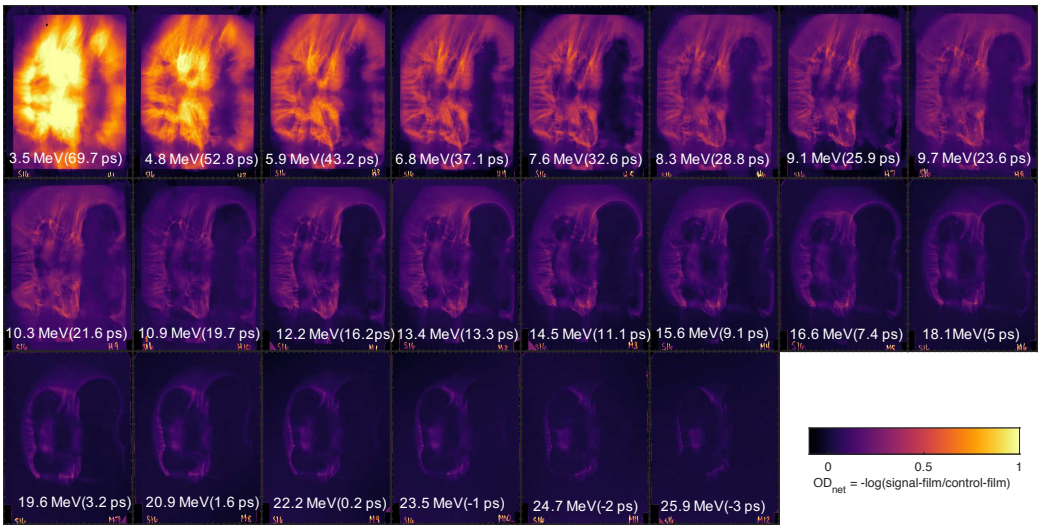

(b) N190523-002

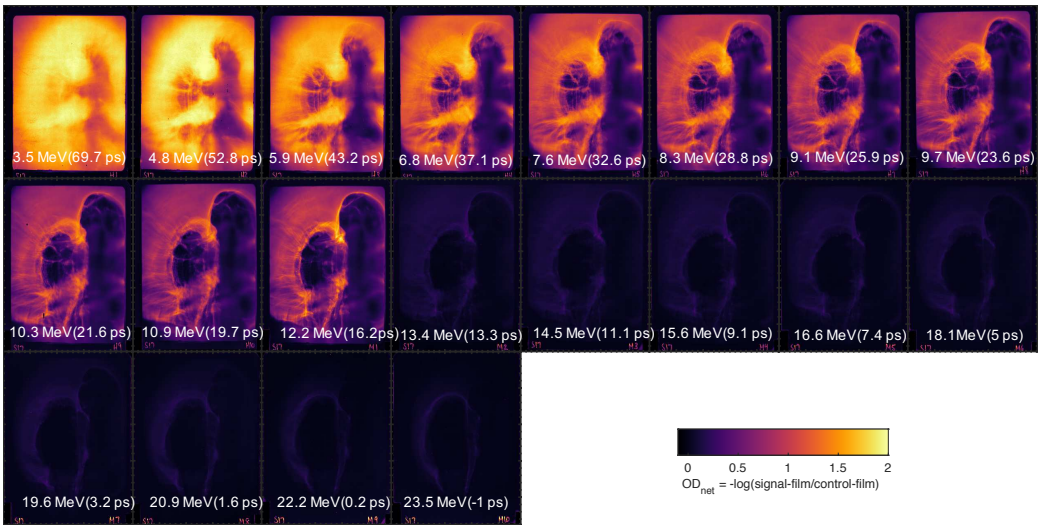

Figure 2. RCF films are shown for the shot with the focusing wedge in (a) and without the focusing wedge in (b). Units of the RCF intensity are in optical density, which is defined as $OD = -log(signal_{film}/control_{film})$, where the control film refers to the signal from an unexposed RCF film. In all radiographs shown here, the green channel was used for the signal film, since as shown Chen *et al.* [24] showed that this channel was the most consistent in terms of absolute value across different RCF scanners. The border of each film was blocked by the RCF pack holder and thus was used here to estimate the signal of an unexposed film.

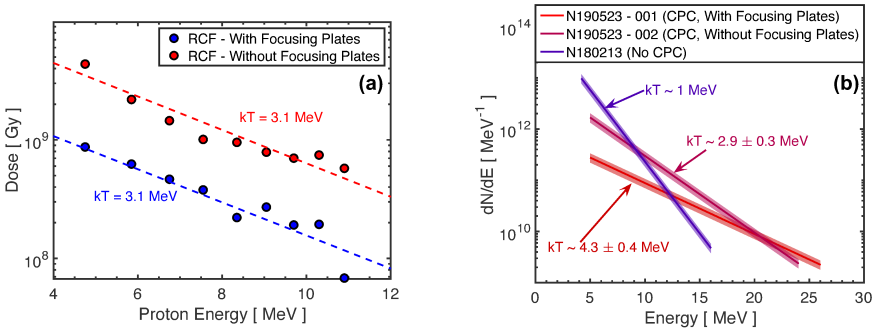

Figure 3. In (a) Dose measurement for each RCF layer for Shot N190523-001 (blue) and Shot N190523-002 (red) derived for the HD-V2 layers of the corresponding RCF stacks. A proton slope temperature (of an exponential form) was also fit to both, which allows for a representation of the proton spectral shape. In (b), the proton spectra was unfolded assuming a one-temperature Boltzmann distribution for N190523-001 and N190523-002. For comparison, a previous shot N180213 is also shown that was also for the purpose of proton acceleration on the NIF-ARC, but was performed using a flat foil target and no CPC. The fitted distributions are plotted up to the maximum proton energies recorded on the RCF as shown in Figure 2

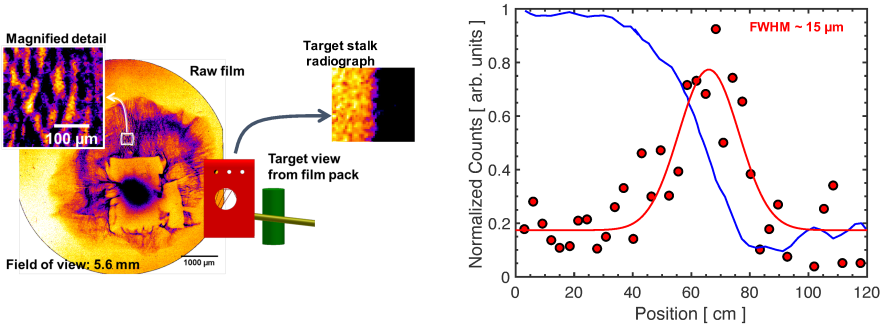

Figure 4. Source size was estimated from a companion shot, where a target stalk holder was used as a first-order knife-edge source size measurement. Details of the companion shot as well as the measured source size are show. The blue curve is the measured edge-spread-function (ESF) and the red markers is the derivative of this blue curve, or the point-spread function (PSF). This PSF is then fit with a gaussian (shown in the solid red curve) and the FWHM of the PSF was roughly 15 microns.

This procedure was performed with the two shots shown in Figure 3(b) for N190523-001 and N190523-002. In addition, the spectra for a previous proton acceleration shot on the NIF-ARC (N180213) with flat foils and no CPC, first reported in Mariscal *et al.*, is shown for comparison in blue. In comparing both spectra, the CPCs appear to make the spectrum both hotter in terms of spectral temperature when compared to proton acceleration on the NIF-ARC without CPCs. This gives further motivation for using CPCs on this platform for the purpose of TNSA proton radiography. Calculating a conversion efficiency, which defined here as $\frac{\int_0^{E_{max}} \frac{dN}{dE} E dE}{E_{Laser}}$, gives a conversion efficiency of 0.7% for N190523-001 (With Focusing Plates) and 2.4% for N190523-002 (Without

Focusing Plates). The conversion efficiency for N180213, the previous shot day without CPCs had a reported conversion efficiency of approximately 1.5%. Interestingly, despite the similar shapes between the two shots with CPCs, the overall proton dose is lower with the focusing plates than without the focusing plates. This remains an open question, but may be due to variability in the CPCs itself between shots and thus warrants more work in this area.

3.2. Source Size Characterization of Proton Probe

Source sizes of radiography sources are often characterized using a knife-edge technique, where a source is directed on an object with a sharp edge [27]. At the image plane there will be a sharp gradient in the signal since the knife-edge will occlude all signal. At the boundary one can take a lineout of this gradient to produce an edge-spread-function (ESF) similar to an error function in shape. The derivative of this edge-spread-function is a point-spread-function (PSF) and the full-width-half-maximum (FWHM) of this PSF can be taken as a source size. To characterize the source size of the NIF-ARC generated proton probe, we used a companion shot (Shot ID: N191006-002-999) where features in the physics package on this experiment could act as a knife-edge to do this measurement. More specifically, a cylindrical stalk that was used to hold a target was in the radiography field-of-view and allowed for an in-situ source size measurement. Taking a line-out of the gradient of this stalk produced the ESF shown in blue in Figure 4 and the PSF from taking the derivative is shown in red. Using this procedure yields a source size of $\sim$15 μm. This figure likely represents an upper limit of the resolution since the stalk is not an optimal knife-edge target for this type of measurement and the image magnification in this setup was 14. Despite this, the measured radiography spatial resolution is still impressive since for comparison, implosion radiography sources are typically $\sim$50 microns and TNSA proton radiography sources at comparable facilities have been shown to be approximately $\sim$10 μm [5].

In terms of our measurement, we can use the measured source size to estimate the geometric source size of the proton beam at the point of interaction (3 mm from the proton probe source) with the physics package. Assuming this FWHM of 15 μm and that the proton beam has a solid angle of 1-steradian, which is typical of TNSA proton sources [7], the beam size at the interaction is 9 mm^2.

4. Conclusions

CPCs have been demonstrated to increase the effective coupling of the NIF-ARC laser to targets, leading to increased TNSA proton energies when compared to TNSA proton experiments on this platform with just a flat foil. Given the higher than anticipated proton energies, future experiments will be conducted to measure the absolute maximum proton energy on the NIF-ARC system as well improve the source size measurement. However, as a lower limit, these experiments demonstrated a maximum proton energy

of at least 26 MeV with spatial resolutions of at least 15 μm. Excitingly, these characteristics are sufficient for now increasing the applications for proton probing on NIF-ARC. Furthermore, high quality radiographs were obtained and demonstrate that this platform is mature enough to be used for a wide variety of HED science applications.

Acknowledgements

The authors would like to thank the NIF-ARC facility staff and scientists for without their expertise the experiment detailed here would not have been possible. We would also like to thank the Discovery Science program at Lawrence Livermore National Laboratory under which this experimental time was allocated. This work was completed under the auspices of the U.S. Department of Energy by Lawrence Livermore National Laboratory under contract DE-AC52-07NA27344 with funding support from the Laboratory Directed Research and Development Program under tracking code 17-ERD-039 and 20-ERD-048, the DOE Office of Science Early Career Research Program under SCW1651, and the Department of Energy National Nuclear Security Administration Laboratory Residency Graduate Fellowship program, which is provided under grant numbers DE-NA0003864 and DE-NA0003960. Support for targets were provided by General Atomics under contract DE-NA0001808. This document was prepared as an account of work sponsored by an agency of the United States government. Neither the United States government nor Lawrence Livermore National Security, LLC, nor any of their employees makes any warranty, expressed or implied, or assumes any legal liability or responsibility for the accuracy, completeness, or useful- ness of any information, apparatus, product, or process disclosed, or represents that its use would not infringe privately owned rights. Reference herein to any specific commercial product, process, or service by trade name, trademark, manufacturer, or otherwise does not necessarily constitute or imply its endorsement, recommendation, or favoring by the United States government or Lawrence Livermore National Security, LLC. The views and opinions of authors expressed herein do not necessarily state or reflect those of the United States government or Lawrence Livermore National Security, LLC, and shall not be used for advertising or product endorsement purposes.

Finally, the authors would like to thank Professor David Neely for his helpful discussions, innovative insight and his enthusiastic and kind support. We dedicate this paper to his memory.

Data Availability Statement

The data that support the findings of this study are available upon reasonable request from the authors.

References

[1] M. J.-E. Manuel, A. B. Zylstra, H. G. Rinderknecht, D. T. Casey, M. J. Rosenberg, N. Sinenian, C. K. Li, J. A. Frenje, F. H. Séguin, and R. D. Petrasso. Source characterization and modeling development for monoenergetic-proton radiography experiments on omega. *Review of Scientific Instruments*, 83(6):063506, 2012.

[2] J. R. Rygg, F. H. Séguin, C. K. Li, J. A. Frenje, M. J.-E. Manuel, R. D. Petrasso, R. Betti, J. A. Delettrez, O. V. Gotchev, J. P. Knauer, D. D. Meyerhofer, F. J. Marshall, C. Stoeckl, and W. Theobald. Proton radiography of inertial fusion implosions. *Science*, 319(5867):1223–1225, 2008.

[3] C. K. Li, F. H. Séguin, J. A. Frenje, M. Rosenberg, R. D. Petrasso, P. A. Amendt, J. A. Koch, O. L. Landen, H. S. Park, H. F. Robey, R. P. J. Town, A. Casner, F. Philippe, R. Betti, J. P. Knauer, D. D. Meyerhofer, C. A. Back, J. D. Kilkenny, and A. Nikroo. Charged-particle probing of x-ray–driven inertial-fusion implosions. *Science*, 327(5970):1231–1235, 2010.

[4] A. J. Mackinnon, P. K. Patel, R. P. Town, M. J. Edwards, T. Phillips, S. C. Lerner, D. W. Price, D. Hicks, M. H. Key, S. Hatchett, S. C. Wilks, M. Borghesi, L. Romagnani, S. Kar, T. Toncian, G. Pretzler, O. Willi, M. Koenig, E. Martinolli, S. Lepape, A. Benuzzi-Mounaix, P. Audebert, J. C. Gauthier, J. King, R. Snavely, R. R. Freeman, and T. Boehlly. Proton radiography as an electromagnetic field and density perturbation diagnostic (invited). *Review of Scientific Instruments*, 75(10):3531–3536, 2004.

[5] A. B. Zylstra, C. K. Li, H. G. Rinderknecht, F. H. Séguin, R. D. Petrasso, C. Stoeckl, D. D. Meyerhofer, P. Nilson, T. C. Sangster, S. Le Pape, A. Mackinnon, and P. Patel. Using high-intensity laser-generated energetic protons to radiograph directly driven implosions. *Review of Scientific Instruments*, 83(1):013511, 2012.

[6] R. A. Snavely, M. H. Key, S. P. Hatchett, T. E. Cowan, M. Roth, T. W. Phillips, M. A. Stoyer, E. A. Henry, T. C. Sangster, M. S. Singh, S. C. Wilks, A. MacKinnon, A. Offenberger, D. M. Pennington, K. Yasuike, A. B. Langdon, B. F. Lasinski, J. Johnson, M. D. Perry, and E. M. Campbell. Intense high-energy proton beams from petawatt-laser irradiation of solids. *Phys. Rev. Lett.*, 85:2945–2948, Oct 2000.

[7] J Fuchs, Patrizio Antici, Emmanuel D'Humières, E. Lefebvre, Marco Borghesi, E Brambrink, C Cecchetti, M Kaluza, Victor Malka, M. Manclossi, S. Meyroneinc, Paola Mora, Jörg Schreiber, Toma Toncian, Henri Pépin, and Patrick Audebert. Laser-driven proton scaling laws and new paths towards energy increase. *Nature Physics*, 2, 01 2006.

[8] J. Schreiber, P. R. Bolton, and K. Parodi. Invited review article: "hands-on" laser-driven ion acceleration: A primer for laser-driven source development and potential applications. *Review of Scientific Instruments*, 87(7):071101, 2016.

[9] Marco Borghesi. Laser-driven ion acceleration: State of the art and emerging mechanisms. *Nuclear Instruments and Methods in Physics Research Section A: Accelerators, Spectrometers, Detectors and Associated Equipment*, 740:6–9, 2014. Proceedings of the first European Advanced Accelerator Concepts Workshop 2013.

[10] C. A. J. Palmer, P. T. Campbell, Y. Ma, L. Antonelli, A. F. A. Bott, G. Gregori, J. Halliday, Y. Katzir, P. Kordell, K. Krushelnick, S. V. Lebedev, E. Montgomery, M. Notley, D. C. Carroll, C. P. Ridgers, A. A. Schekochihin, M. J. V. Streeter, A. G. R. Thomas, E. R. Tubman, N. Woolsey, and L. Willingale. Field reconstruction from proton radiography of intense laser driven magnetic reconnection. *Physics of Plasmas*, 26(8):083109, 2019.

[11] L. Romagnani, M. Borghesi, C.A. Cecchetti, S. Kar, P. Antici, P. Audebert, S. Bandhoupadjay, F. Ceccherini, T. Cowan, J. Fuchs, and et al. Proton probing measurement of electric and magnetic fields generated by ns and ps laser-matter interactions. *Laser and Particle Beams*, 26(2):241–248, 2008.

[12] J. M. Di Nicola, S. T. Yang, C. D. Boley, John K. Crane, J. E. Heebner, Thomas M. Spinka, P. Arnold, C. P. J. Barty, M. W. Bowers, T. S. Budge, K. Christensen, J. W. Dawson, G. Erbert,

E. Feigenbaum, G. Guss, C. Haefner, M. R. Hermann, Doug Homoelle, J. A. Jarboe, J. K. Lawson, R. Lowe-Webb, Kathleen P. McCandless, Brent McHale, L. J. Pelz, P. P. Pham, M. A. Prantil, M. L. Rehak, M. A. Rever, Michael C. Rushford, R. A. Sacks, M. Shaw, D. Smauley, L. K. Smith, R. Speck, G. Tietbohl, P. J. Wegner, and C. Widmayer. The commissioning of the advanced radiographic capability laser system: experimental and modeling results at the main laser output. In Abdul A. S. Awwal and Monya A. Lane, editors, *High Power Lasers for Fusion Research III*, volume 9345, pages 122 – 133. International Society for Optics and Photonics, SPIE, 2015.

[13] D. Mariscal, T. Ma, S. C. Wilks, A. J. Kemp, G. J. Williams, P. Michel, H. Chen, P. K. Patel, B. A. Remington, M. Bowers, L. Pelz, M. R. Hermann, W. Hsing, D. Martinez, R. Sigurdsson, M. Prantil, A. Conder, J. Lawson, M. Hamamoto, P. Di Nicola, C. Widmayer, D. Homoelle, R. Lowe-Webb, S. Herriot, W. Williams, D. Alessi, D. Kalantar, R. Zacharias, C. Haefner, N. Thompson, T. Zobrist, D. Lord, N. Hash, A. Pak, N. Lemos, M. Tabak, C. McGuffey, J. Kim, F. N. Beg, M. S. Wei, P. Norreys, A. Morace, N. Iwata, Y. Sentoku, D. Neely, G. G. Scott, and K. Flippo. First demonstration of arc-accelerated proton beams at the national ignition facility. *Physics of Plasmas*, 26(4), 4 2019.

[14] Andrew G. MacPhee, David Alessi, Hui Chen, Ginevra Cochran, Mark R. Hermann, Daniel H. Kalantar, Andreas J. Kemp, Shaun M. Kerr, Anthony J. Link, Tammy Ma, Andrew J. Mackinnon, Derek A. Mariscal, David Schlossberg, Riccardo Tommasini, Scott Vonhof, Clifford C. Widmayer, Scott C. Wilks, G. Jackson Williams, Wade H. Williams, and Kelly Youngblood. Enhanced laser–plasma interactions using non-imaging optical concentrator targets. *Optica*, 7(2):129–130, Feb 2020.

[15] G. J. Williams, A. Link, M. Sherlock, D. A. Alessi, M. Bowers, B. P. Golick, M. Hamamoto, M. R. Hermann, D. Kalantar, K. N. LaFortune, A. J. Mackinnon, A. MacPhee, M. J.-E. Manuel, D. Martinez, M. Mauldin, L. Pelz, M. Prantil, M. Quinn, B. Remington, R. Sigurdsson, P. Wegner, K. Youngblood, and Hui Chen. Order-of-magnitude increase in laser-target coupling at near-relativistic intensities using compound parabolic concentrators. *Phys. Rev. E*, 103:L031201, Mar 2021.

[16] D. R. Rusby, P. M. King, A. Pak, N. Lemos, S. Kerr, G. Cochran, I. Pagano, A. Hannasch, H. Quevedo, M. Spinks, M. Donovan, A. Link, A. Kemp, S. C. Wilks, G. J. Williams, M. J.-E. Manuel, Z. Gavin, A. Haid, F. Albert, M. Aufderheide, H. Chen, C. W. Siders, A. Macphee, and A. Mackinnon. Enhancements in laser-generated hot-electron production via focusing cone targets at short pulse and high contrast. *Phys. Rev. E*, 103:053207, May 2021.

[17] A.B. Zylstra, J.R. Rygg, G.W. Collins, C.K. Li, J.A. Frenje, R.D. Petrasso, S.R. Nagel, P. Fitzsimmons, and H. Reynolds. Platform development for de/dx measurements on short-pulse laser facilities. *High Energy Density Physics*, 35:100731, 2020.

[18] P. K. Patel, A. J. Mackinnon, M. H. Key, T. E. Cowan, M. E. Foord, M. Allen, D. F. Price, H. Ruhl, P. T. Springer, and R. Stephens. Isochoric heating of solid-density matter with an ultrafast proton beam. *Phys. Rev. Lett.*, 91:125004, Sep 2003.

[19] R. A. Snavely, B. Zhang, K. Akli, Z. Chen, R. R. Freeman, P. Gu, S. P. Hatchett, D. Hey, J. Hill, M. H. Key, Y. Izawa, J. King, Y. Kitagawa, R. Kodama, A. B. Langdon, B. F. Lasinski, A. Lei, A. J. MacKinnon, P. Patel, R. Stephens, M. Tampo, K. A. Tanaka, R. Town, Y. Toyama, T. Tsutsumi, S. C. Wilks, T. Yabuuchi, and J. Zheng. Laser generated proton beam focusing and high temperature isochoric heating of solid matter. *Physics of Plasmas*, 14(9):092703, 2007.

[20] M. Roth, D. Jung, K. Falk, N. Guler, O. Deppert, M. Devlin, A. Favalli, J. Fernandez, D. Gautier, M. Geissel, R. Haight, C. E. Hamilton, B. M. Hegelich, R. P. Johnson, F. Merrill, G. Schaumann, K. Schoenberg, M. Schollmeier, T. Shimada, T. Taddeucci, J. L. Tybo, F. Wagner, S. A. Wender, C. H. Wilde, and G. A. Wurden. Bright laser-driven neutron source based on the relativistic transparency of solids. *Phys. Rev. Lett.*, 110:044802, Jan 2013.

[21] C McGuffey, J Kim, M S Wei, P M Nilson, S N Chen, J Fuchs, P Fitzsimmons, M E Foord, D Mariscal, H S McLean, P K Patel, R B Stephens, and F N Beg. Focussing Protons from a

Kilojoule Laser for Intense Beam Heating using Proximal Target Structures. *Scientific Reports*, 10(1):9415, 2020.

[22] S. R. Nagel, T. J. Hilsabeck, P. M. Bell, D. K. Bradley, M. J. Ayers, M. A. Barrios, B. Felker, R. F. Smith, G. W. Collins, O. S. Jones, J. D. Kilkenny, T. Chung, K. Piston, K. S. Raman, B. Sammuli, J. D. Hares, and A. K. L. Dymoke-Bradshaw. Dilation x-ray imager a new/faster gated x-ray imager for the nif. *Review of Scientific Instruments*, 83(10):10E116, 2012.

[23] A. J. Kemp and S. C. Wilks. Direct electron acceleration in multi-kilojoule, multi-picosecond laser pulses. *Physics of Plasmas*, 27(10):103106, 2020.

[24] S. N. Chen, M. Gauthier, M. Bazalova-Carter, S. Bolanos, S. Glenzer, R. Riquier, G. Revet, P. Antici, A. Morabito, A. Propp, M. Starodubtsev, and J. Fuchs. Absolute dosimetric characterization of gafchromic ebt3 and hdv2 films using commercial flat-bed scanners and evaluation of the scanner response function variability. *Review of Scientific Instruments*, 87(7):073301, 2016.

[25] Graeme Gordon Scott. private communication.

[26] F. Nürnberg, M. Schollmeier, E. Brambrink, A. Blažević, D. C. Carroll, K. Flippo, D. C. Gautier, M. Geißel, K. Harres, B. M. Hegelich, O. Lundh, K. Markey, P. McKenna, D. Neely, J. Schreiber, and M. Roth. Radiochromic film imaging spectroscopy of laser-accelerated proton beams. *Review of Scientific Instruments*, 80(3):033301, 2009.

[27] E. Gumbrell, J. M. McNaney, C. M. Huntington, A. G. Krygier, and H.-S. Park. Characterizing the modulation transfer function for x-ray radiography in high energy density experiments. *Review of Scientific Instruments*, 89(10):10G118, 2018.